Development/Plasticity/Repair

The *stat3/socs3a* Pathway Is a Key Regulator of Hair Cell Regeneration in Zebrafish *stat3/socs3a* Pathway: Regulator of Hair Cell Regeneration

Jin Liang,[1,3] Dongmei Wang,[4] Gabriel Renaud,[1] Tyra G. Wolfsberg,[1] Alexander F. Wilson,[2] and Shawn M. Burgess[1]

[1]Genome Technology Branch, and [2]Inherited Disease Research Branch, National Human Genome Research Institute, Bethesda, Maryland 20892, [3]Neuroscience and Cognitive Science Program, University of Maryland, College Park, Maryland 20742, and [4]Qingdao Institute of BioEnergy and BioProcess Technology, Chinese Academy of Sciences, Qingdao 266101, Shandong, People's Republic of China

All nonmammalian vertebrates studied can regenerate inner ear mechanosensory receptors (i.e., hair cells) (Corwin and Cotanche, 1988; Lombarte et al., 1993; Baird et al., 1996), but mammals possess only a very limited capacity for regeneration after birth (Roberson and Rubel, 1994). As a result, mammals experience permanent deficiencies in hearing and balance once their inner ear hair cells are lost. The mechanisms of hair cell regeneration are poorly understood. Because the inner ear sensory epithelium is highly conserved in all vertebrates (Fritzsch et al., 2007), we chose to study hair cell regeneration mechanism in adult zebrafish, hoping the results would be transferrable to inducing hair cell regeneration in mammals. We defined the comprehensive network of genes involved in hair cell regeneration in the inner ear of adult zebrafish with the powerful transcriptional profiling technique digital gene expression, which leverages the power of next-generation sequencing ('t Hoen et al., 2008). We also identified a key pathway, *stat3/socs3*, and demonstrated its role in promoting hair cell regeneration through stem cell activation, cell division, and differentiation. In addition, transient pharmacological inhibition of *stat3* signaling accelerated hair cell regeneration without overproducing cells. Taking other published datasets into account (Sano et al., 1999; Schebesta et al., 2006; Dierssen et al., 2008; Riehle et al., 2008; Zhu et al., 2008; Qin et al., 2009), we propose that the *stat3/socs3* pathway is a key response in all tissue regeneration and thus an important therapeutic target for a broad application in tissue repair and injury healing.

Introduction

The sensory epithelium of the inner ear is mainly composed of two types of cells: hair cells and supporting cells (Fritzsch et al., 2006). Inner ear hair cells are the basic mechanosensory receptors for hearing and balance (Vollrath et al., 2007), while supporting cells provide a variety of functions including being the stem cells for replacing hair cells in most vertebrates (Balak et al., 1990; Baird et al., 1996; Jones and Corwin, 1996). All nonmammalian vertebrates studied show the ability to regenerate their inner ear hair cells (Cruz et al., 1987; Corwin and Cotanche, 1988; Lombarte et al., 1993; Baird et al., 1996). However, in mammals, loss of inner ear hair cells caused by acoustic overexposure (McGill and Schuknecht, 1976), otoxic drugs (Lim, 1976) or aging (Soucek et al., 1986) is the major cause of permanent auditory and vestibular deficiencies because mammals lose regenerative ability after birth (Roberson and Rubel, 1994). Because the inner ear sensory epithelium is highly conserved in all vertebrates (Fritzsch et al., 2007), numerous studies have been done in nonmammalian vertebrates to understand the mechanism of hair cell regeneration (Brignull et al., 2009). However, our understanding of the mechanisms involved is still very limited because it is a complex, multistaged process (Stone and Cotanche, 2007).

In this study, we used the powerful profiling technique digital gene expression (DGE) ('t Hoen et al., 2008; Morrissy et al., 2009) to study the hair cell regeneration in zebrafish at high resolution to get a more comprehensive view of the process. In zebrafish, spontaneous and damage-induced hair cell production has been demonstrated in both the inner ear (Bang et al., 2001; Higgs et al., 2002; Schuck and Smith, 2009) and the neuromasts (Harris et al., 2003), a mechanosensory structure highly similar to the sensory epithelia of the inner ear (Nicolson, 2005) and thus an excellent model for studying hair cell regeneration (Harris et al., 2003; Hernández et al., 2007; Ma et al., 2008; Behra et al., 2009). In addition, zebrafish are commonly used as a genetic/genomic model organism, making zebrafish a valuable system for studying the molecular mechanisms of hair cell regeneration in adult vertebrates in a systematic fashion.

By analyzing the expression profiles from inner ear tissues during regeneration, we identified a key pathway, *stat3/socs3*, and demonstrated its role in promoting regeneration. Signal transducer and activator of transcription 3 (*stat3*) is a transcription

Received Nov. 3, 2010; revised June 12, 2012; accepted June 13, 2012.

Author contributions: J.L., D.W., and S.M.B. designed research; J.L. and D.W. performed research; G.R. and T.G.W. contributed unpublished reagents/analytic tools; J.L., D.W., G.R., T.G.W., A.F.W., and S.M.B. analyzed data; J.L. and S.M.B. wrote the paper.

This research was supported by the Intramural Research Program of the National Human Genome Research Institute, National Institutes of Health (S.M.B.). We thank A. Popper for use of the sound exposure equipment and helpful discussions, and D. Bodine and W. Pavan for critical reading of the manuscript.

This article is freely available online through the *J Neurosci* Open Choice option.

The authors declare no competing financial interests.

Correspondence should be addressed to Shawn M. Burgess at the above address. E-mail: burgess@mail.nih.gov.

DOI:10.1523/JNEUROSCI.5785-10.2012

 0270-6474/12/3210662-12$15.00/0

factor. Its downstream targets include *stat3* itself and suppressor of cytokine signaling 3 (*socs3*) (Leonard and O'Shea, 1998). Socs3 protein antagonizes the activation of Stat3 in the cytosol as a negative feedback (Leonard and O'Shea, 1998). The self-restrictive pathway is known to be involved in the following various biological processes: cell proliferation, cell migration, immune responses, cell survival (Yoshimura, 2009; Yu et al., 2009), as well as regeneration in skin (Sano et al., 1999; Zhu et al., 2008), liver (Dierssen et al., 2008; Riehle et al., 2008), fins (Schebesta et al., 2006), and retinas (Qin et al., 2009). Comparing our data with those in other publications, we propose that the *stat3*/*socs3* pathway is a key response in all tissue regeneration and thus a potential therapeutic target for tissue repair.

Materials and Methods

Animal husbandry. Zebrafish were maintained under approved animal protocols as previously described (Westerfield, 2000) and in compliance with guidelines for animal care from NIH and the University of Maryland.

Noise exposure of adult zebrafish. Adult wild-type TAB-5 (Amsterdam et al., 1999) mixed-sex zebrafish (~1 year old) were exposed to white noise (100–10,000 Hz, 150–170 dB re 1 μPa) for 48 h at 28–29°C according to a protocol modified from Smith et al. (2006). After exposure, the fish were maintained under regular husbandry conditions until killed. The control fish were not exposed to noise.

Tag profiling and tag mapping. The tag profiling data of inner ear tissues were generated by Illumina. Tags detected only once were discarded. The tag sequences were mapped against transcriptome and genomic sequence databases: Refseq RNAs, UniGene, Ensembl RNAs, Ensembl RNA *ab initio*, and the zebrafish genome (Zv.8). UniGene IDs were used as the primary index (except for those Refseq RNAs without corresponding UniGene IDs). The expression level of a certain gene (identified by a unique UniGene ID) was the summation of counts of the tags that were "unambiguously mapped" to the gene normalized by the total counts of all tags obtained in the profile in the expression unit called transcripts per million.

Analyses of expression profiling data. The sample clustering analysis was done using Genesifter software (Geospiza). Candidate genes were identified for further analysis if they showed significant differences in expression level during regeneration compared with the control sample (i.e., ≥1.5-fold increase or ≥2-fold decrease in expression level with a p value <0.01, as determined by χ^2 test or Fisher's exact test. Pathway analysis was done with MetaCore software (GeneGo).

Quantitative RT-PCR. Glyceraldehyde-3-phosphate dehydrogenase (GAPDH) and bactin1 were used as reference genes. The relative change in expression level of a gene X in an experimental sample compared with the control sample was calculated as $2 \times (\Delta Ct_{EXPx} - \Delta Ct_{CONx})$, where $\Delta Ct_{EXPx} = (Ct_{EXPref} - Ct_{EXPx})$ and $\Delta Ct_{CONx} = (Ct_{CONref} - Ct_{CONx})$. Ct is the cycle number at which amplification rises above the background threshold. All primers are listed in Table 1.

Whole-mount in situ *hybridization.* Regular whole-mount *in situ* hybridization (ISH) of zebrafish embryos was done as previously described (Oxtoby and Jowett, 1993). Fluorescent whole-mount *in situ* hybridization was performed according to the regular *in situ* hybridization protocol, except that the TSA Cyanine 3 system (PerkinElmer) was used for developing fluorescent signals. All primers for probe synthesis are listed in Table 1.

Morpholino and mature mRNA injection. The injections were done in fertilized eggs of TAB-5 (Amsterdam et al., 1999) or *Tg(cldnb:GFP)* (Haas and Gilmour, 2006) lines. Morpholinos (MOs) against *stat3*, *socs3a*, and *tp53* (Table 1) were injected at a concentration of 500 μM. The mature mRNA of *socs3a* was injected at a concentration of 37.8 ng/μl.

Induction of lateral line hair cell death in larval zebrafish. The 5 d post-fertilization (dpf)-old larval fish were treated with 10 μM $CuSO_4$ for 2 h at 28.5°C as previously described (Hernández et al., 2007) to induce complete lateral line hair cell loss.

Quantification of hair cell numbers and mitotic events during lateral line hair cell regeneration. After $CuSO_4$ treatment to induce lateral line hair cell death, 5-dpf-old *Tg(pou4f3:GFP)* larvae (Xiao et al., 2005) were then raised at 28.5°C in the Holtfreter's buffer containing S3I-201 (400 μM, EMD Biosciences) or DMSO (40 μl/10 ml buffer, Sigma). Lateral line hair cells (GFP-positive cells) in living larvae were quantified at 24, 48, and 72 h post-treatment (hpt). The mitotic events during lateral line hair cell regeneration were quantified by a bromodeoxyuridine (BrdU) incorporation assay (Ma et al., 2008).

Table 1. Sequences of primers and morpholinos

Experiment	Target gene	Sequence
qRT-PCR	*atoh1a*	F: 5′-GCG AAG AAT GCA CGG ATT GAA CCA-3′
		R: 5′-TGC AGG GTT TCG TAC TTG GAG AGT-3′
	bactin1	F: 5′-GAC CCA GAC ATC AGG GAG TGA TGG-3′
		R: 5′-AGG TGT GAT GCC AGA TCT TCT CCA TG-3′
	bcl6	F: 5′-TGT TCT GCT CAA CCT GAA CCG ACT-3′
		R: 5′-TAG AAG AGC CCA CTG CAT GCC ATA-3′
	dld	F: 5′-TCC AAC CCT TGC TCG AAT GAT GCT-3′
		R: 5′-TCG ATG TTG TCT TCG CAG TGC GTT-3′
	gapdh	F: 5′-ACT CCA CTC ATG GCC GTT AC-3′
		R: 5′- TGA GCT GAG GCC TTC TCA AT-3′
	jak1	F: 5′-ACG AGT GCT TGG GAA TGG CTG TTT-3′
		R: 5′-AGT TGC GTT GCT TAA TGG TGC GGT-3′
	mmp2	F: 5′-GCT GGT GTG CAA CCA CTG AAG ATT-3′
		R: 5′-AAG ACA CAG GGT GCT CCA TCT GAA-3′
	mmp9	F: 5′-AAA TCG AGA AGC TCG GCC TAC CAA-3′
		R: 5′- TCC TCT GTC AAT CAG CTG AGC CTT-3′
	socs3a	F: 5′-TAA AGC AGG GAA GAC AAG AGC CGA-3′
		R: 5′-TGG AGA AAC AGT GAG AGA GCT GGT-3′
	socs3b	F: 5′-CGG ATA ACG CTT TGA AGC TGC CTT-3′
		R: 5′-TAC TAT GCG TTA CCA TGG CGC TCT-3′
	stat3	F: 5′-AGT GAA AGC AGC AAA GAG GGA GGA-3′
		R: 5′-TGA GCT GCT GCT TAG TGT ACG GTT-3′
In situ hybridization probe synthesis	*stat3*	F: 5′-**ATT AAC CCT CAC TAA AGG GA**C GCA AGT TCA ACA TCC TTG GCA CT-3′
		R: 5′-**TAA TAC GAC TCA CTA TAG GGA GA**T TTG GCT CGG AGA GAG AAA GCA GT-3′
	socs3a	F: 5′-**ATT AAC CCT CAC TAA AGG GA**A AGA CTG TGA ACG GAC ACA CGG AT-3′
		R: 5′-**TAA TAC GAC TCA CTA TAG GGA GA**A GTG TCT GGC ATG AGA AGG CTG AA-3′
Morpholino	*socs3a*	M01: CCCTGAGCTGCCGGGAAGCAGATCT
		M02: CGTGTAATATACAGAGTGTCGAGTC
	stat3	M01: GCCATGTTGACCCCTTAATGTGTCG
	tp53	M01: GCGCCATTGCTTTGCAAGAATTG

A list of primers for qRT-PCR and *in situ* hybridization probe synthesis are listed. The bold sequences are T3 [forward (F)] and T7 [reverse (R)] promoters included in the primers for probe synthesis. Both morpholinos targeting *socs3a* gave rise to similar phenotypes. Results in the article are from embryos injected with M01. *stat3* MO was synthesized based on sequences from Yamashita et al. (2002), which was also used by Sepich et al. (2005) and Kassen et al. (2009) for knocking down *stat3* expression in zebrafish embryos. *tp53* MO was synthesized based on sequences from Kratz et al. (2006).

Immunohistochemistry. The primary and secondary antibodies used include the rabbit myosin VI and myosin VIIa antibodies (1:200 dilution, Proteus Biosciences), rabbit anti-stat3^{pS727} (1:50 dilution, Abcam), mouse anti-BrdU with Alexa Fluor 546 conjugate (1:200 dilution, Invitrogen), goat GFP antibody (FITC conjugated, 1:200 dilution, Abcam), and Alexa Fluor 568 (or 488) goat anti-rabbit IgG (1:1000 dilution, Invitrogen). The inner ear sensory epithelia were dissected as previously described (Liang and Burgess, 2009).

Microscopy and image analysis. To capture images of the entire saccular epithelia, several overlapping pictures were taken for each epithelium with Zeiss Vision software and tiled with Photoshop 7.0 software (Adobe). The imaging in the living larvae was done using an Axiovert200M and an Apotome Grid Confocal (Zeiss). The antibody staining and fluorescent *in situ* hybridization results of embryos/larvae were visualized under AxiovertNLO confocal microscope (Zeiss) with Zeiss AIM software. The regular *in situ* hybridization results were captured using a Leica MZ16F microscope with Leica FireCam software.

Statistical analysis. χ^2 tests (genes with tag count >5) and Fisher's exact tests (genes with tag count ≤5) were used to compare the expres-

sion levels of the genes quantified by tag profiling. The calculation was done using R software. Expression data from inner ear samples collected at different time points during regeneration were compared with those from the control sample. One-way ANOVA, *post hoc* test, and Student's *t* test were used to compare hair cell numbers. The calculations were done using Excel software (Microsoft).

Results

Inner ear hair cell regeneration in adult zebrafish

We induced inner ear hair cell loss in adult zebrafish by modifying a previously published noise exposure protocol (Smith et al., 2006) (Fig. 1*A*). Using this setup, we could consistently induce hair cell loss in the anterior-medial region of the saccular macula (Fig. 1*B*), but not in the utricular or lagenar macula (data not shown), which is consistent with the proposed function of saccule as the major auditory end organ in otophysians (Fay, 1978). We confirmed complete elimination of the hair cells (as opposed to hair cell bundle damage) with phalloidin (staining hair cell bundles) and myosin VI/VIIa antibodies (staining hair cell bodies) (Fig. 1*C*). When we quantified the hair cells in a 20 × 20 μm area at 40% of the total length of the anterior–posterior axis of the epithelium at 24 h intervals from 0 to 120 h postexposure (hpe), we found that the hair cells regrew rapidly and returned to control levels in 96 h (Fig. 1*C*,*D*), consistent with a previous publication (Schuck and Smith, 2009).

Candidate gene/pathway identification by DGE

Based on the time line of hair cell regeneration in adult fish (Fig. 1*C*,*D*), we collected inner ear tissue samples at 0, 24, 48, and 96 hpe and generated the expression profiles from the samples using the DGE tag-profiling technique (Morrissy et al., 2009). The raw data from profiling included sequences of 944,347 unique tag sequences (20 nt) and a "count" associated with each tag sequence (Table 2). The count is a direct quantification of the copy number of the transcript that the tag represents. The total count number of all the tag sequences was 15,744,948. After filtering the raw data (see Materials and Methods), we mapped 303,342 unique tags from a total of 15,103,943 sequences to transcriptome and genome databases (Table 2). Approximately 60% of the tags were mapped to at least one known/predicted transcript or at least one location on the genome (Fig. 2*A*). Although ~40% of the unique tag sequences failed to be mapped, the total proportion of unmapped tags only accounted for ~7.2% of the total tag counts. When one mismatch was allowed during the mapping, only ~7% of the tag sequences failed to be mapped, suggesting that the failure in mapping most likely resulted from sequencing errors and/or single-nucleotide polymorphisms. In this study, we adopted conservative criteria, only analyzing tags with no mismatch in mapping and matching to a single UniGene entry.

A total of 80,604 unique tags were unambiguously mapped to a known/predicted transcript (Fig. 2*A*) (i.e., the tag could be assigned to one and only one of the known/predicted transcripts). Those 80,640 tags were used for gene identification and expression level calculations. Clustering analysis of the five expression profiles with Genesifter (Geospiza) software based on the calculation of the overall differences between profiles showed that the 96 hpe profile shared the highest similarity with the control profile, followed by the 24 hpe and the 48 hpe profiles, which were highly similar to each other, and then by a 0 hpe profile that differed the most from the control profile (Fig. 2*C*, top). Essentially the transcriptional profiles were most different immediately after noise exposure and slowly returned to normal over the course of 4 d.

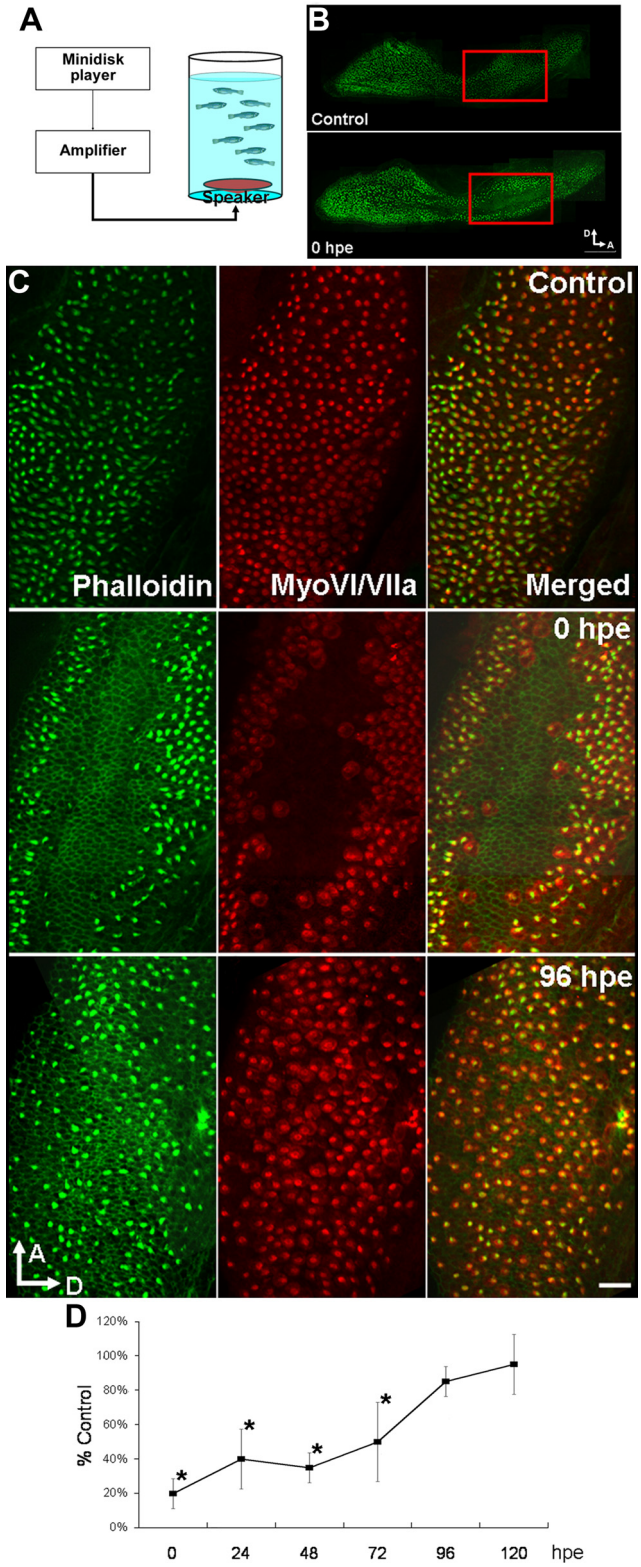

Figure 1. Saccular hair cells were eliminated by noise exposure and subsequently regenerated. ***A***, Hair cell loss in the saccule was consistently induced by the noise exposure apparatus. ***B***, Phalloidin staining of the saccular hair cells; hair cell loss occurred in the anterior-medial area of the saccular sensory epithelium (red boxes; scale bar, 100 μm). ***C***, Closer examination of the damaged area with phalloidin (green channel) and anti-myosin VI/VIIa (red channel) staining confirmed the complete elimination of hair cell bodies (middle; scale bar, 20 μm) as well as the repopulation of hair cells to control level by 96 hpe in the damaged area (bottom). ***D***, Quantification of hair cell number after sound exposure (one-way ANOVA and *post hoc* test, $n = 3$, $^*p < 0.05$; all error bars in this publication demonstrate SD). D, Dorsal; A, anterior.

Table 2. Summary of tag profiling results

	Total		After filtration	
	Count	Unique tag	Count	Unique tag
Control	3,339,753	327,240	3,199,598	187,085
0 hpe	2,758,836	279,532	2,646,064	166,760
24 hpe	3,615,956	317,505	3,486,384	187,933
48 hpe	3,476,027	331,687	3,337,409	193,069
96 hpe	2,554,376	289,177	2,434,488	169,289
Total	15,744,948	944,347	15,103,943	303,342

The numbers of tag counts and unique tag sequences from each of the five expression profiles in raw data (under the "Total" column) and after the removal of the tag sequences that were detected only once in five profiles (under the "After filtration" column).

We used χ^2 tests and Fisher's exact tests to compare the expression level of each gene during regeneration to the control level. A total of 2269 genes with significant changes in their expression levels at one or more time points during regeneration were identified as candidate genes (data available upon request). Measureable changes in expression levels detected by DGE were confirmed in several candidate genes (selected because of already known functions in hair cell development or because of direct interest in the genes) with quantitative RT-PCR (qRT-PCR) (Fig. 2*B*). We performed a pathway analysis for the 2269 candidate genes using the Metacore (GeneGo) software package. The functions of the most enriched interaction network calculated from the candidate genes in each experimental time point are listed in Figure 2*C* (bottom). While the enriched pathways identified by Metacore were generally broad, the fact that the different collected time points had very different enrichment profiles, indicated distinct phases in the regeneration process. The results of profile distance calculation and enrichment analysis corresponded nicely with the distinct morphological changes in the saccular epithelium during regeneration, as well as with the known cellular mechanisms during hair regeneration in other nonmammalian vertebrates (Stone and Cotanche, 2007).

Because we were interested in identifying early signaling events that trigger regeneration, we prioritized our candidates for functional analysis from the highly enriched networks that were apparent at the earliest measured time point (0 hpe, Fig. 2*D*). Metacore and Pathway Studio both identified a large interconnected pathway with the hub of that pathway centering on *stat3* (Fig. 2*D*). Confirming the potential importance, the gene *socs3a* (a zebrafish homolog of human *SOCS3*), a downstream target of *stat3* (and a negative-feedback inhibitor for *stat3* activity) was one of the largest transcriptional changes at 0 hpe (≈10-fold increase). By 24 hpe, *stat3* and *socs3a* signaling return to normal levels, suggesting that this response is an important early regenerative response but is not necessary in later stages of regeneration. With the help of the analysis, we identified the *stat3*/*socs3* pathway as the dominant signaling pathway to become activated at the earliest time point of recovery with >50 relevant genes in the pathway responding to hair cell damage (Fig. 2*D*). No other known signaling pathway had as many connected nodes as the *stat3*/*socs3a* node in the 0 hpe responses. Related genes in the *stat3*/*socs3* pathway, such as *socs3b* (a paralog of *socs3a* in zebrafish), Janus kinase 1 (*jak1*), and matrix metalloproteinase 9 (*mmp9*), also showed significant changes in their expression levels (Fig. 2*B*; data available on request).

Self-restrictive feedback between *stat3* and *socs3a* in zebrafish

In mammals, there is a self-restrictive feedback mechanism between *stat3* and *socs3*: *stat3* activates the transcription of *socs3,* which in turn, antagonizes *stat3* activation (Leonard and O'Shea, 1998). To test whether there is a similar feedback mechanism between *stat3* and *socs3a* in zebrafish, we temporarily knocked down *stat3* or *socs3a* in zebrafish embryos using MO injection. We detected a decrease in the mRNA levels of both *stat3* and *socs3a* in *stat3* morphants but an increase in the mRNA levels of both genes in *socs3a* morphants (Table 3). This is the expected result for a negative-feedback loop. To further confirm the knock-down studies, we injected mature mRNA of *socs3a* to zebrafish embryos and found a reduction in *stat3* expression level, mimicking the effects of *stat3*-MO injection (Table 3). These data demonstrate that the self-restrictive feedback relation between *stat3* and *socs3a* in mammals is maintained in zebrafish.

The stat3/socs3a pathway is involved in hair cell production in zebrafish development

In addition to the hair cells in their inner ears, zebrafish, like other fishes and amphibians, also possess the mechanosensory lateral line organ for detecting water movement over the body (Montgomery et al., 2000; McHenry et al., 2009). The neuromasts in the lateral line are composed of hair cells and supporting cells that are highly similar to those in the inner ear sensory epithelium (Nicolson, 2005). In addition, the hair cell regeneration in the lateral line neuromasts shares a similar molecular mechanism to that in the inner ear (Harris et al., 2003; Ma et al., 2008; Behra et al., 2009).

Both *stat3* (Oates et al., 1999; Thisse and Thisse, 2004) and *socs3a* (Fig. 3*A*) are expressed in the neuromasts at 5 dpf, implying a normal function in those tissues for either development or homeostasis. In addition, *stat3* is known to be expressed in the anterior region of the otic vesicle at earlier developmental stages (Oates et al., 1999; Thisse and Thisse, 2004). As an initial test of the roles for *stat3* and *socs3* in hair cell regeneration, we tested the effects of morpholino inhibition of each gene on normal inner ear development. Testing two different morpholinos for *socs3a* and a previously published and verified one for *stat3* (Yamashita et al., 2002), knocking down *stat3* or *socs3a* had a clear inhibitory effect on hair cell production (Fig. 3*B–E*). In *stat3* morphants, the anterior otolith in the otic vesicles was often missing while the posterior otolith appeared approximately normal (Fig. 3*B*). Correspondingly, a closer examination of the maculae in the otic vesicle revealed a significantly decreased number of hair cells in the anterior macula in those morphants while the hair cell number in the posterior macula remained normal (Fig. 3*C*,*D*). Coinjection with *tp53* MO resulted in an identical phenotype (data not shown), suggesting that the hair cell-related phenotypes are gene specific. The phenotypes of the morphants corresponded nicely with the expression pattern of both genes detected by *in situ* hybridization (Oates et al., 1999; Thisse and Thisse, 2004) (Fig. 3*A*). The phenotypes also serve as an indirect confirmation of the involvement *stat3*/*socs3* pathway in hair cell regeneration, as hair cell production during development and regeneration will, to some extent, share similar genetic programs (Stone and Rubel, 1999; Cafaro et al., 2007; Ma et al., 2008; Daudet et al., 2009).

To further understand the function of the *stat3*/*socs3* pathway in hair cell production, we measured the mRNA level of atonal homolog 1a (*atoh1a*) in *stat3* and *socs3a* morphants. *atoh1a* is one of the zebrafish homologs of *atoh1*, an essential gene required for hair cell fate commitment (Bermingham et al., 1999; Woods et al., 2004; Millimaki et al., 2007). Both the knocking down of *stat3* and the overexpression of *socs3a* resulted in a reduction in *atoh1a* mRNA level (Table 3) but did not change the overall distribution or timing of expression based on *in situ* hybridization (data not shown). In contrast, a strong increase in *atoh1a* mRNA level was

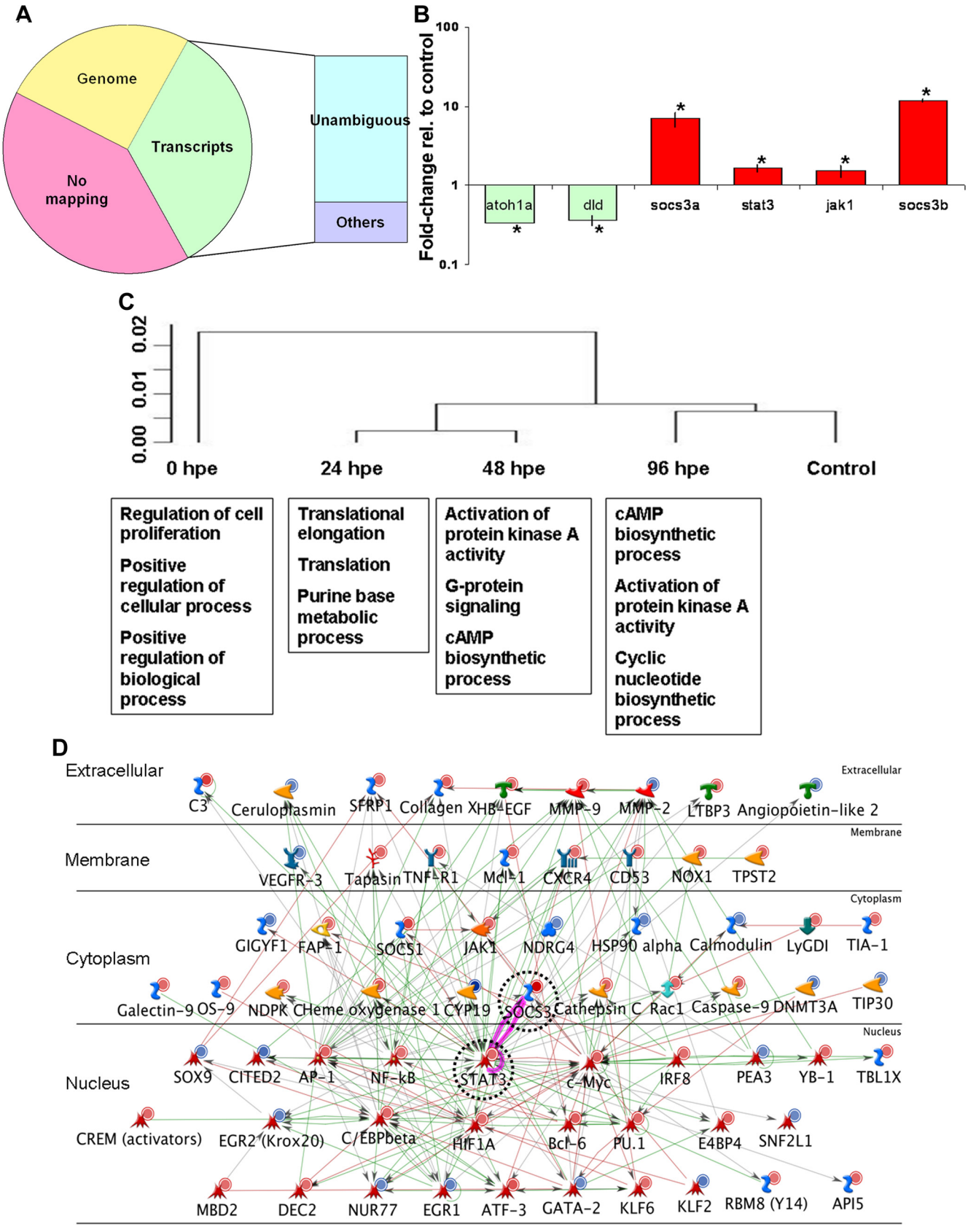

Figure 2. Analyses and confirmation of tag-profiling results from inner ear tissues collected during hair cell regeneration. ***A***, A total number of 303,342 unique-sequence tag sequences from inner ear tissues collected at five time points were mapped against transcriptome and genome databases. Approximately 34% of the tag sequences were mapped to one or more known/predicted transcripts and ~17% to unique loci in genome (without a known transcript), leaving ~49% of the sequences without transcriptome or genome mapping. Among those tags mapped to known/predicted transcripts, ~78% were unambiguously mapped. ***B***, Some of the candidate genes (0 hpe) identified by tag profiling were confirmed by qRT-PCR using GAPDH (*Figure legend continues.*)

Table 3. Summary of qRT-PCR results in morpholino- and mRNA-injected embryos

	Target gene		
	Atoh1a	*Stat3*	*Socs3a*
socs3a MO (36 hpf)	1.35 (9.91e-3)	1.76 (0.0284)	8.37 (0.0324)
socs3a mRNA (12 hpf)	0.615 (2.70e-3)	0.720 (0.0235)[a]	
stat3 MO (32 hpf)	0.547 (0.0105)	0.294 (1.77e-4)	0.600 (0.041)

In developing embryos, *stat3* and *socs3a* were knocked down respectively with MO injection, and *socs3a* was also temporarily overexpressed with mRNA injection. Changes in mRNA levels of *atoh1a*, *stat3*, and *socs3a* in MO/mRNA-injected embryos compared to control embryos were determined with qRT-PCR. The numbers in each cell stand for fold change and *p* value (in braces).

[a]Data collected from a 6 hpf embryo.

observed in *socs3a* morphants where *stat3* was hyperactivated (Table 3), demonstrating that *stat3*/*socs3a* are positive/negative regulators of *atoh1a* expression. In addition, the cross talk between *stat3*/*socs3* and *atoh1* was further confirmed by *in situ* hybridization of the *socs3a* morphants (Fig. 3*E*). At 24 and 36 hpf, there is little detectable difference in *atoh1a* expression between *socs3a* morphants and wild-type fish by *in situ* hybridization (data not shown). But at 48 and 72 hpf, there is a clear expansion of *atoh1a* expression in the otic vesicle (Fig. 3*E*, arrowhead), the hindbrain, and the spinal chord (Fig. 3*E*, bracket), suggesting the *stat3*–*atoh1a* regulatory relationship is not unique to the sensory epithelia of the inner ear and lateral line, but is a more general pathway for regulation. These results suggest that the *stat3*/*socs3* pathway is involved in the hair cell differentiation process possibly by directly or indirectly expanding *atoh1a* expression.

Stat3 activation during hair cell regeneration and development in lateral line neuromasts

Because the lateral line neuromasts are located on the surface of the body, it makes the lateral line a convenient model for testing hair cell regeneration. Expression of both *stat3* (Thisse and Thisse, 2004) and *socs3a* (Fig. 3*A*) was detected in the neuromasts at 5 dpf, so we continued with additional functional studies of the *stat3*/*socs3a* pathway during regeneration in larval neuromasts. At 5 dpf, the number of hair cells in the lateral line neuromasts reaches a relatively stable level (Ma et al., 2008; Behra et al., 2009), which enables us to differentiate regeneration of hair cells from normal growth and development.

We induced hair cell death in the lateral line neuromasts with $CuSO_4$, a protocol ensuring complete lateral line hair cell elimination within 2 h in 5 dpf larvae (Hernández et al., 2007), which is followed subsequently by regeneration of hair cells to control levels within 72 h (Behra et al., 2009). We performed *in situ* hybridization in larval fish after 2 h of $CuSO_4$ treatment and found an increase in the level of *stat3* expression in the lateral line neuromasts when hair cell death was induced (Fig. 4*A*). In addition, we also found changes in the location of *stat3* expression induced by $CuSO_4$-triggered hair cell death (Fig. 4*A*), which was further confirmed by fluorescent whole-mount *in situ* hybridization in *ET20* larvae that marks the mantle cells of the neuromasts with GFP expression the outermost layer of nonsensory cells in the neuromast (Parinov et al., 2004) (Fig. 4*B*). RNA probes against *stat3* were mostly detected in the GFP-positive cells of the neuromasts in untreated *ET20* larvae (Fig. 4*B*, top). When hair cell death was induced, *stat3* expression was no longer limited to the mantle cells, but was expressed strongly throughout the supporting cells of the neuromasts. The *in situ* hybridization data confirmed the activation of *stat3* induced by hair cell death in the lateral line neuromasts was in the supporting cell population, matching expression increases observed by DGE during inner ear hair cell regeneration.

The activation of mammalian *stat3* protein is mostly characterized by the phosphorylation of either Y705 (Yoshimura, 2009; Yu et al., 2009) or S727, which functions concurrently with Y705 (Wen et al., 1995) or independently (Liu et al., 2003; Qin et al., 2008). The corresponding amino acid (S751) and the flanking amino acid sequences are highly conserved in zebrafish *stat3* when compared with the human protein, so we first tracked the activation of *stat3* in the neuromasts after $CuSO_4$ treatment with an antibody that recognizes STAT3 S727 phosphorylation ($STAT3^{pS727}$). We found a significant increase in $STAT3^{pS727}$-positive nuclei in the neuromasts at 12 hpt with $CuSO_4$ in the $CuSO_4$-treated larvae relative to control (Fig. 4*A*,*B*). Double labeling with GFP in *Tg(scm1:GFP)* (Behra et al., 2009) demonstrates that the cells with nuclear staining of $STAT3^{pS727}$ are the supporting cells (Fig. 4*A*). The activation and the nuclear import of *stat3* protein in the supporting cells subsequent to hair cell death indicate the activation of *stat3* signaling during hair cell regeneration.

Hair cell production during development and regeneration will, to some extent, share similar genetic programs (Stone and Rubel, 1999; Cafaro et al., 2007; Ma et al., 2008; Daudet et al., 2009), so we checked whether *stat3* activation in the lateral line neuromasts is similar during development and regeneration. In 3 dpf larvae, most cells in the neuromasts showed homogeneous $STAT3^{pS727}$ labeling only in their nuclei (Fig. 5*A*′, top). Double-labeling with *scm1*:GFP demonstrates that those cells are supporting cells (Fig. 5*A*′, top). In addition, in differentiating hair cells, the nuclear labeling of $STAT3^{pS727}$ antibody decreased and became spotty, with cytoplasmic labeling becoming predominant, suggesting that the *stat3* was becoming inactive in these cells (Fig. 5*A*′, top, close-ups). The nuclear import of *stat3* in supporting cells during hair cell regeneration in 5 dpf and older larvae seems to be recapitulating the *stat3* activation during immature neuromast development in younger larvae.

It is noteworthy that in older larvae, a significant level of labeling was still detectable in a subgroup of mantle cells that are marked by GFP in the ET20 transgenic line (Fig. 5*A*′, bottom). The significance of this cell population having activated *stat3* is not yet clear, but it seems to represent a distinct cellular compartment in the lateral line neuromasts.

Inhibition of *stat3*-promoted hair cell regeneration

To further clarify the function of *stat3*, we compared the hair cell regeneration processes with and without the presence of a *stat3* inhibitor. The majority of the chemical inhibitors were ototoxic and could not be used for regeneration studies (data not shown). One published inhibitor, S3I-201, was not toxic on its own and was used to test the role of *stat3* in hair cell regeneration. S3I-201

←

(*Figure legend continued.*) as a reference gene ($n = 3$, one-tailed *t* test, $*p = 1.81e\text{-}4, 3.78e\text{-}4, 9.41e\text{-}3, 8.76e\text{-}3, 0.0272, 1.578e\text{-}4$). ***C***, Clustering analysis of the five expression profiles with Genesifter showed the relationship between different profiles (top diagram). The clustering results had the predicted relationship where the 0 hpe expression was the most different from control and then the samples progressively returned to "normal" over time. Pathway analysis showed cell signaling pathways represented by the candidate genes that are critical for specific phases of regeneration [e.g., cell proliferation-related at 0 hpe and cell differentiation-related at later time points (bottom boxes)]. ***D***, Pathway analysis of the candidate genes (identified at 0 hpe) involved in inner ear hair cell regeneration highlighted the interactions between *stat3* and *socs3* (dashed circles) with other identified candidate genes. The known interactions (red: positive; green: negative; gray: unspecified) between the human orthologs of the candidate genes were extracted in batches to predict the candidate pathways involved in the hair cell regeneration. Different colors of the circles indicate those genes being upregulated (red) or downregulated (blue) during hair cell regeneration.

is a cell-permeable chemical that binds to the SH2 domain of mammalian *stat3* protein and reportedly blocks the dimerization of phosphorylated (activated) *stat3* molecules (Siddiquee et al., 2007). After exposing *Tg(pou4f3:GFP)* larvae (in which the hair cells are labeled with GFP) (Xiao et al., 2005) to $CuSO_4$, we quantified the regenerating hair cells and performed a BrdU incorporation assay (Ma et al., 2008). The S3I-201-treated larvae showed a significant increase in BrdU incorporation in the neuromasts compared with DMSO-treated larvae (control) at 24 hpt, but not at 48 or 72 hpt (Fig. 6*A*). Accordingly, the S3I-201-treated larvae had more hair cells per neuromast at 48 hpt, but not at 24 or 72 hpt (Fig. 6*A*), which is consistent with an expected lag between supporting cell division and subsequent hair cell differentiation. In essence, the hair cells regenerated faster in the S3I-201-treated embryos than in controls. Similar results were observed when hair cell quantification was done by myosin VI antibody staining (data not shown). S3I-201 did not have a significant impact on hair cell numbers in larvae that had not been treated with $CuSO_4$ (data not shown).

To confirm the inhibitory function of S3I-201 in hair cell regeneration triggered by $CuSO_4$ ototoxicity, we performed ISH to examine the mRNA levels of *stat3* and *socs3a* in the lateral line neuromasts after 1 h of $CuSO_4$ treatment with or without the presence of S3I-201. The ISH data demonstrated a reduction in both *stat3* (Fig. 6*B*) and *socs3a* (Fig. 6*B′*) expression in the neuromasts cotreated with both $CuSO_4$ and S3I-201 compared with those treated only with $CuSO_4$. Our qRT-PCR results were in accordance with the ISH results in that *stat3* expression in larvae treated with both $CuSO_4$ and S3I-201 was only 81% of the level in larvae treated only with $CuSO_4$ ($p = 0.0014$, $n = 3$ for both groups). Since stat3 activates its own expression, the data suggest that S3I-201 stimulated hair cell regeneration by moderately inhibiting *stat3* activity.

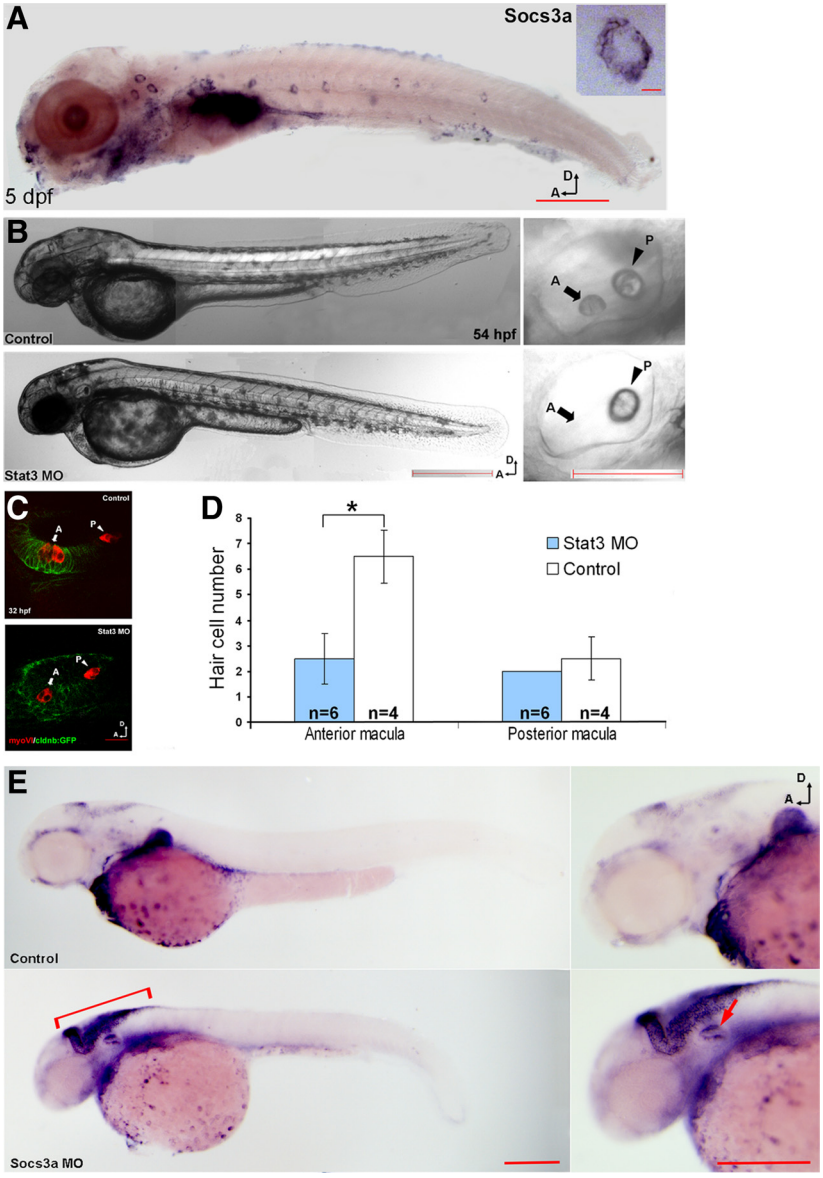

Figure 3. *stat3* and *socs3a* are involved in hair cell production during zebrafish larval development. ***A***, *socs3a* expression was detected in anterior and posterior lateral line neuromasts in 5 dpf larvae by *in situ* hybridization; there is a close-up of one neuromast in the top right corner (scale bars: top, 10 μm; bottom, 1 mm). Expression of *socs3a* is similar to *stat3* expression (Oates et al., 1999; Thisse and Thisse, 2004). ***B***, The anterior otolith (arrows labeled with "A") in *stat3* morphants was typically missing, while the posterior otolith (arrowheads labeled with "P") appeared approximately normal (scale bars: left, 500 μm; right, 100 μm). ***C***, MyosinVI antibody staining (red channel) of the hair cells in the anterior sensory macula (arrows labeled with A) and posterior macula (arrowheads labeled with P) in control larvae and *stat3* morphants (scale bar, 20 μm) at 32 hpf. *cldnb*:GFP (green channel) was used to outline the otic vesicle. ***D***, The *stat3* morphants showed a significant reduction in the number of hair cells in the anterior macula, but not in the posterior macula at 32 hpf ($n = 4$ (control)/6 (MOs), one-tailed *t* test, $*p = 2.79e\text{-}4$). ***E***, Both *stat3* and *socs3a* morphants possessed fewer posterior lateral line neuromasts ($n = 10$ in all groups, one-tailed *t* test, $*p = 2.52e\text{-}08$, 2.41e-04) with a smaller number of hair cells per neuromast ($n = 10$ in all groups, one-tailed *t* test, $*p = 1.10e\text{-}06$, 1.56e-10) compared with control larvae at 2.5 dpf. In *socs3a* morphants (bottom), an expansion of *atoh1a* expression was detected by *in situ* hybridization in the brain area (bracket) as well as the otic vesicle (arrow) compared with control (top) (scale bars: left, 1 mm; right, 500 μm). D, Dorsal; A, anterior; MO, morpholino.

Discussion

Recent studies have demonstrated the power of using the DGE platform for measuring transcriptional changes ('t Hoen et al., 2008; Morrissy et al., 2009). Using DGE, we generated a comprehensive list of candidate genes involved in the inner ear hair cell regeneration in adult zebrafish (data available upon request). One major pathway that is initiated in the earliest responses centers on *stat3* and *socs3a*. This pathway is broadly implicated in the initial signaling responses of hair cell regeneration in the zebrafish inner ear. We went on to show that *stat3*/*socs3* signaling played an important role in cell division and hair cell differentiation during both normal development and tissue regeneration.

Stat3 signaling: activated during development and regeneration

To some extent, hair cell production during both development and regeneration share similar genetic programs (Stone and Rubel, 1999; Cafaro et al., 2007; Ma et al., 2008; Daudet et al.,

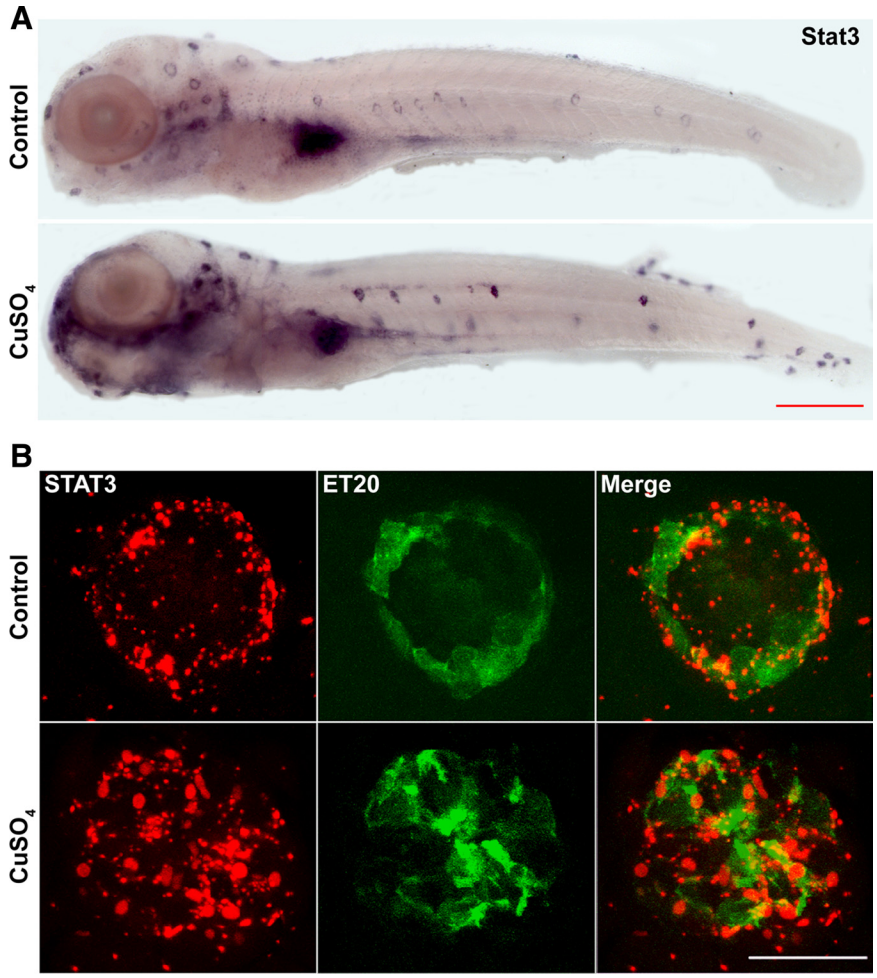

Figure 4. Hair cell death in the lateral line system resulted in an increase in *stat3* expression level in the nonsensory cells in the neuromasts. ***A***, The results of regular whole-mount *in situ* hybridization targeting *stat3* mRNA in control (top) $CuSO_4$-treated (bottom) larvae showed an increase in *stat3* expression when hair cell death took place. Scale bar, 1 mm. ***B***, Costaining of neuromasts with fluorescent detection of probes targeting *stat3* mRNA (red channel) and FITC-conjugated anti-GFP antibody (green channel) in *ET20* transgenic larvae showed an increase in nonsensory cells in the neuromasts after hair cell death. Scale bar, 20 μm.

2009). In this study, we identified *stat3* and *socs3a* as important regulators in zebrafish hair cell regeneration in the inner ear (data available upon request) and lateral line system (Fig. 5*A*). Correspondingly, we also found them required for normal hair cell production during the larval development (Fig. 3*B–E*). The examination of *stat3* activity in lateral line neuromasts during development and regeneration further confirms the similarity shared between the two processes. Activated, nuclear-localized *stat3* protein was detected in a large number of supporting cells and differentiating hair cells in 3 dpf larvae (Fig. 5*A′*) and was downregulated in those same cells in the neuromasts of more mature 5 dpf larvae (Fig. 5*A*). However, when hair cell death was triggered in 5 dpf larvae, the *stat3* protein was again activated and imported into the nuclei of the supporting cells (Fig. 5*A*), recapitulating the active *stat3* observed during neuromast development (Fig. 5*A′*).

Another interesting observation is the specific overlap of $STAT3^{pS727}$-positive cells and the GFP-positive mantle cells of *ET20* larvae (Fig. 5*A′*), which is further supported by the enrichment of *stat3* mRNA in those GFP-positive cells (Fig. 4*A*). This suggests that the mantle cells have a specific function in the neuromast that requires activated *stat3*. Previous publications suggest two types of stem cell-like cells in the neuromasts, one type involved in long-term cell replacement (i.e., the true stem cells), and the other in an amplification/differentiation role (Williams and Holder, 2000; Ma et al., 2008). The role of the ET20:GFP-labeled (and *stat3*-activated) mantle cells may regulate the cell division of adjacent stem cells through a nonautonomous mechanism similar to the role of *stat92E* in escort cells for regulating the stem cell division in the *Drosophila* ovary (Decotto and Spradling, 2005). These ET20:GFP and $STAT3^{pS721}$-positive cells would represent part of the niche environment necessary to promote normal cell turnover as well as tissue regeneration. Alternatively, the mantle cells might directly divide asymmetrically to repopulate the supporting cells of the neuromasts after damage or cell turnover. The triggering of cell differentiation seemed to be achieved, at least in part, through activation of *atoh1* (Fig. 3*E*), a key regulator of hair cell differentiation (Fig. 7). This pathway seems to be used in more than one tissue type as *socs3a* inhibition results in an expansion of *atoh1a* expression in both the otic vesicle and in the brain. It is noteworthy that while *atoh1a* expression is expanded in the otic vesicle with a hyperactive *stat3*, the number of hair cells was not (data not shown), suggesting that more factors are necessary for hair cell differentiation.

A previous microarray study did show basal-level expression of *stat3* in newborn rat cochlea that could be elevated by stress in explant cultures (Gross et al., 2008). It was also reported that *stat3* showed a temporal expression pattern similar to *gata2* and *C/EBP* during the *in vitro* differentiation of conditional cell lines derived from mouse otocyst (Holley et al., 2007). Little is known about the functions of *stat3* and *socs3* in the inner ear in mammals other than that activated *stat3* protein is detected in the outer hair cells in mouse cochlea late in embryonic development (Hertzano et al., 2004). The persistence of *stat3* expression in a subset of supporting cells in zebrafish that is not detected in the mammalian cochlea might represent a key difference that enables nonmammalian vertebrates to regenerate hair cells. A more detailed comparison study focusing on the *stat3*/*socs3* signaling pathway in the inner ears in mice and zebrafish would help us further understand key regulators of hair cell regeneration. In addition, it is also intriguing to explore whether cell cycle progression can be triggered in supporting cells by genetic and/or pharmacological enhancement of *stat3* activity in damaged mammalian sensory epithelia.

The *stat3*/*socs3* pathway may serve as a common initiator in a variety of regenerative processes

The *stat3*/*socs3* pathway is best known as the mediator of a wide variety of biological processes, including cell proliferation, cell migration, immune response, and cell survival (Yoshimura,

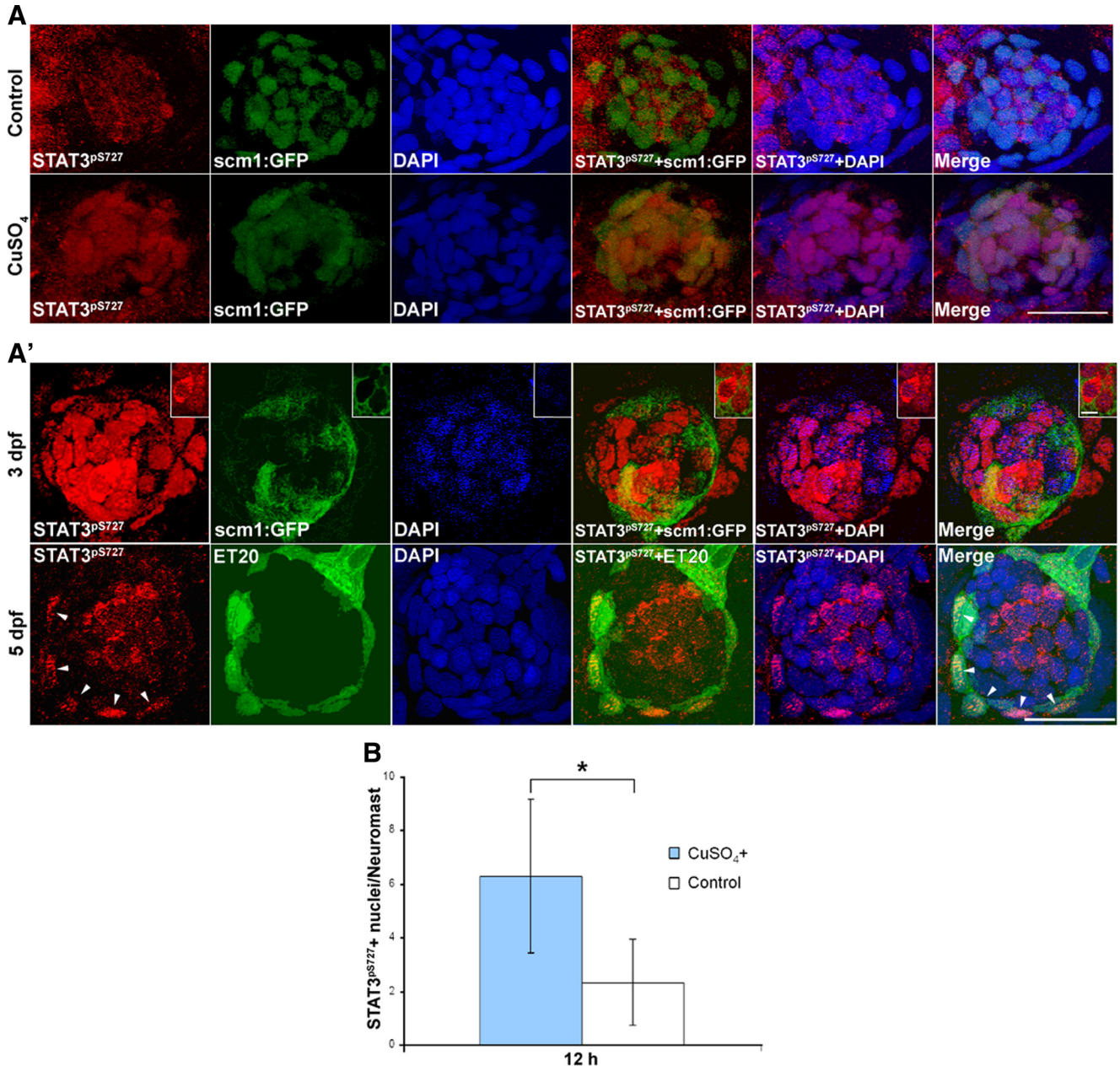

Figure 5. Phosphorylation and nuclear import of *stat3* proteins were detected in the regenerating and developing neuromasts. ***A***, Costaining of anti-STAT3 ^{pS727} with DAPI in *Tg(scm1:GFP)* larvae confirmed anti-STAT3 ^{pS727} labeling mainly in the nuclei of supporting cells (GFP positive) at 12 hpt with copper compared with untreated controls. Scale bar, 20 μm. ***A'***, In 3 dpf larvae, the majority of the supporting cell nuclei (GFP-positive cells) were labeled with STAT3 ^{pS727} antibody (top). Differentiating hair cells showed decreased STAT3 ^{pS727} nuclear staining, but an increase of STAT3 ^{pS727} labeling in the cytoplasm (top, close-ups; scale bar: close-ups, 5 μm). Nuclear anti-STAT3 ^{pS727} labeling decreased dramatically in more mature neuromasts in 5 dpf larvae (bottom), except for a small group of cells labeled with GFP (arrowheads) in *ET20* transgenic larvae (scale bars, 20 μm). ***B***, Quantification of activated phospho-STAT3. The increase in nuclear localized phospho-*stat3* was statistically significant ($n = 10/9$, one-tailed t test, $p = 9.83e\text{-}4$). S727 in human STAT3 corresponds to S751 in zebrafish STAT3 by sequence alignment.

2009; Yu et al., 2009). Studies in mouse skin (Sano et al., 1999; Zhu et al., 2008) and liver (Dierssen et al., 2008; Riehle et al., 2008) further confirm the importance of the *stat3*/*socs3* pathway for proper wound healing. For example, in microarray datasets from other zebrafish regeneration experiments, a strong induction of *socs3* expression was consistently observed during the regeneration of fins (Schebesta et al., 2006) and retinas (Qin et al., 2009). *stat3* expression was also found to be upregulated in dividing cells during zebrafish retinal photoreceptor regeneration (Kassen et al., 2009). The early activation of *stat3* in the supporting cells subsequent to hair cell death is consistent with these previous studies and suggests that this is a common pathway for healing. *stat–jak* signaling has been found to play a critical role in the development and regeneration of the epithelial cells in the *Drosophila* midgut by initiating cell division and inducing differentiation (Jiang et al., 2009), a dual process that is highly similar to what we demonstrated during regeneration of the inner ear sensory epithelia. In zebrafish inner ear and lateral line regeneration, the activation of *stat3* signaling in supporting cells precedes the cell division, suggesting that the gene is playing a role in cell cycle progression of those cells. A recent study supports this idea as it reported leukemia inhibitory factor promoted cell division in a cochlea-derived cell line, HEI-OC1, through the *stat3/jak2* signaling pathway (Chen et al., 2010). This suggests that *stat* signal-

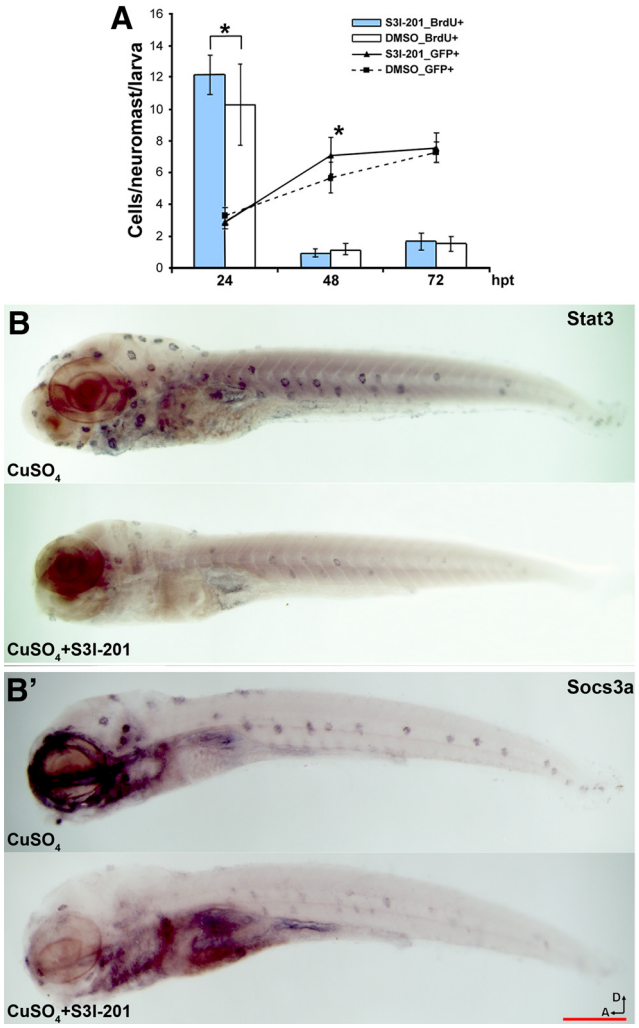

Figure 6. S3I-201 promoted lateral line hair cell regeneration by downregulating *stat3/socs3* signaling. ***A***, Quantification of hair cells after lateral line hair cell loss induced by $CuSO_4$ treatment; larvae incubated with S3I-201 had more hair cells [GFP-positive cells in *Tg(pou4f3:GFP)*] per neuromast at 48 hpt with $CuSO_4$ compared with the control larvae incubated with DMSO ($n = 12/9$, one-tailed *t* test, $*p = 5.34e\text{-}3$), but not at 24 or 72 hpt (line graph). BrdU incorporation assays showed a significantly higher number of BrdU-positive cells per neuromast in larvae incubated with S3I-201 at 24 hpt ($n = 16/10$; one-tailed *t* test, $*p = 9.24e\text{-}3$), but not at later time points (bar graph). ***B***, ***B′***, 5 dpf larvae fish were treated with $CuSO_4$ with or without the presence of S3I-201 for 1 h and examined with *in situ* hybridization. *stat3* (***B***) and *socs3a* (***B′***) expression levels were both reduced in larvae treated with both $CuSO_4$ and S3I-201 (***B*** and ***B′***, top) compared with those treated with only $CuSO_4$ (***B*** and ***B′***, bottom). Scale bar, 1 mm. D, Dorsal; A, anterior.

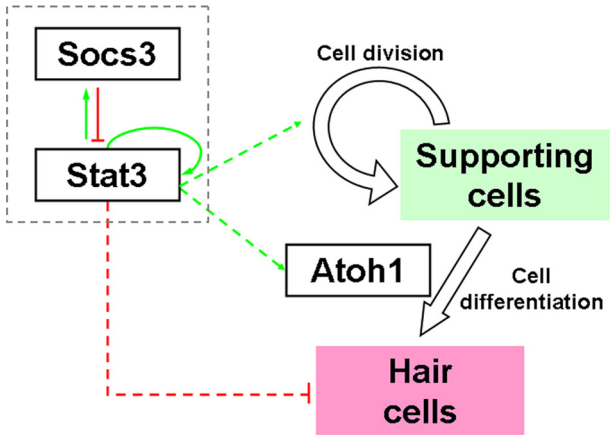

Figure 7. The working model of the *stat3/socs3* pathway and the interaction of *stat3/socs3* with *atoh1* during hair cell regeneration in zebrafish. *stat3* positively regulates the function of *atoh1*, a key player in promoting hair cell fate commitment, in a direct or indirect manner. In addition, the balancing of the *stat3/socs3* pathway is crucial to hair cell differentiation: either hyperactivation or hypoactivation of *stat3* inhibits hair cell differentiation. The self-restrictive loop helps to balance the expression of *stat3* spatially and temporally to ensure the appropriate replenishment of the lost hair cells.

ing is a fundamental initiating mechanism of tissue regeneration that operates through cell division and differentiation and has been conserved for over the 300 million years of evolution from invertebrates to vertebrates. Together, all these data strengthen our hypothesis that *stat3/socs3* is a central activating mechanism of stem cell populations in most, if not all, forms of regeneration.

Although *stat3* activation can be considered as a promoting factor for a regenerative process, we showed that a mild inhibition of *stat3* via a chemical antagonist (Fig. 6*B*, *B′*) could accelerate hair cell regeneration by promoting supporting cell division (Fig. 6*A*). Because *stat3* is also known to be required for the maintenance of pluripotency of various types of stem cells (Raz et al., 1999), and we did identify a small group of putative stem cells in the neuromasts with persisting *stat3* activity under quiescent/undamaged conditions (Fig. 5*A′*), a possible explanation for the observation that inhibiting *stat3* modestly enhanced regeneration at early time points is that S3I-201 forced the premature division and differentiation of these stem cells, resulting in an increase in BrdU incorporation at 24 hpt and in hair cell number at 48 hpt (Fig. 6*A*). However, we do not believe such a mechanism contributed much, if any, to the difference between S3I-201-treated larvae and control larvae during regeneration. First, we observed an accelerated regeneration without overproduction or underproduction of hair cells (Fig. 6*A*), suggesting that we were simply accelerating the normal process. Meanwhile, undamaged larvae raised with S3I-201 from 5 to 8 dpf did not show any significant difference in the number of the lateral hair cells compared with control, showing it was not the release of a cell cycle block in the mantle (ET20-positive) cells that explains the accelerated appearance of the hair cells. In addition, the damage-induced *stat3* activation was observed in all of the supporting cells (Fig. 4*B*), the main source of new hair cells during regeneration (Ma et al., 2008). While we cannot completely rule out the contribution of any other mechanism, the data here do support our hypothesis that S3I-201 promoted the division of the supporting cells through mild downregulation of the damage-induced *stat3* activity in those cells. In essence, S3I-201 increased the rate of *stat3* inactivation that naturally occurs through *socs3a* activation, allowing the cells to proceed to mitosis and cell differentiation sooner.

We believe that our results emphasize the balance of *stat3/socs3* signaling as being crucial for a successful healing process. Two examples in the literature demonstrated that excessive *stat3* activity can block cell cycle progression and inhibit regeneration similar to what we observed; prolonged overexpression of IL-6 and the resulting hyperactivation of *stat3* inhibited regeneration after hepatectomy in mice (Wüstefeld et al., 2000; Jin et al., 2006). Moreover, excessive *stat3* activity in fatty livers was associated with the cell cycle arrest after hepatectomy (Torbenson et al., 2002). Accordingly, keeping the cytokine signaling tempered by the negative feedback of *socs3* is known to be crucial for proper regeneration (Taub, 2004). Tissue-specific knockout of *socs3* in mice led to an upregulation in *stat3* activity but delayed skin wound healing due to the increased neutrophil and macrophage

infiltration and elevated chemokine expression (Zhu et al., 2008). In addition, we are not ruling out the possibility that *stat3* may play more than one role in more than one type of cell in tissue regeneration. It is known that *stat3* is activated in hepatocytes as well as myeloid cells after hepatectomy (Wang et al., 2010). However, while knocking out *stat3* in hepatocytes inhibits cell cycle progression and regeneration, knocking out *stat3* in myeloid cells leads to the opposite results (Wang et al., 2010). Previous data also suggest a complicated cross talk of *stat3* signaling pathway in different cell types during regeneration (Wang et al., 2010). Given the known active involvement of myeloid cells in lateral line hair cell death in zebrafish larvae (d'Alençon et al., 2010), it is very likely that S3I-201 treatment disturbed the *stat3* signaling in not only supporting cells but also myeloid cells and even the cross talk between these two types of cells. Our data together with data from many others demonstrate crucial yet complicated roles of the *stat3*/*socs3* pathway during tissue regeneration. We have developed a model for *stat3* that requires initial activation of *stat3* with a critical negative-feedback role for *socs3a*. Further studies are necessary to work out the exact roles of each gene in this complex and dynamic process. While s*tat3* activation could potentially be therapeutic to injuries in a wide variety of tissues, caution needs to be taken for such application, given the multifaceted functions of *stat3* in the injury and healing process.

References

Amsterdam A, Burgess S, Golling G, Chen W, Sun Z, Townsend K, Farrington S, Haldi M, Hopkins N (1999) A large-scale insertional mutagenesis screen in zebrafish. Gene Dev 13:2713–2724.

Baird RA, Steyger PS, Schuff NR (1996) Mitotic and nonmitotic hair cell regeneration in the bullfrog vestibular otolith organs. Ann NY Acad Sci 781:59–70.

Balak KJ, Corwin JT, Jones JE (1990) Regenerated hair cells can originate from supporting cell progeny: evidence from phototoxicity and laser ablation experiments in the lateral line system. J Neurosci 10:2502–2512.

Bang PI, Sewell WF, Malicki JJ (2001) Morphology and cell type heterogeneities of the inner ear epithelia in adult and juvenile zebrafish (Danio rerio). J Comp Neurol 438:173–190.

Behra M, Bradsher J, Sougrat R, Gallardo V, Allende ML, Burgess SM (2009) Phoenix is required for mechanosensory hair cell regeneration in the zebrafish lateral line. PLoS Genet 5:e1000455.

Bermingham NA, Hassan BA, Price SD, Vollrath MA, Ben-Arie N, Eatock RA, Bellen HJ, Lysakowski A, Zoghbi HY (1999) Math1: an essential gene for the generation of inner ear hair cells. Science 284:1837–1841.

Brignull HR, Raible DW, Stone JS (2009) Feathers and fins: non-mammalian models for hair cell regeneration. Brain Res 1277:12–23.

Cafaro J, Lee GS, Stone JS (2007) Atoh1 expression defines activated progenitors and differentiating hair cells during avian hair cell regeneration. Dev Dyn 236:156–170.

Chen HC, Ma HI, Sytwu HK, Wang HW, Chen CC, Liu SC, Chen CH, Chen HK, Wang CH (2010) Neural stem cells secrete factors that promote auditory cell proliferation via a leukemia inhibitory factor signaling pathway. J Neurosci Res 88:3308–3318.

Corwin JT, Cotanche DA (1988) Regeneration of sensory hair cells after acoustic trauma. Science 240:1772–1774.

Cruz RM, Lambert PR, Rubel EW (1987) Light microscopic evidence of hair cell regeneration after gentamicin toxicity in chick cochlea. Arch Otolaryngol Head Neck Surg 113:1058–1062.

d'Alençon CA, Pena OA, Wittmann C, Gallardo VE, Jones RA, Loosli F, Liebel U, Grabher C, Allende ML (2010) A high-throughput chemically induced inflammation assay in zebrafish. BMC Biol 8:151.

Daudet N, Gibson R, Shang J, Bernard A, Lewis J, Stone J (2009) Notch regulation of progenitor cell behavior in quiescent and regenerating auditory epithelium of mature birds. Dev Biol 326:86–100.

Decotto E, Spradling AC (2005) The Drosophila ovarian and testis stem cell niches: Similar somatic stem cells and signals. Dev Cell 9:501–510.

Dierssen U, Beraza N, Lutz HH, Liedtke C, Ernst M, Wasmuth HE, Trautwein C (2008) Molecular dissection of gp130-dependent pathways in hepatocytes during liver regeneration. J Biol Chem 283:9886–9895.

Fay RR (1978) Phase-locking in goldfish saccular nerve fibres accounts for frequency discrimination capacities. Nature 275:320–322.

Fritzsch B, Pauley S, Beisel KW (2006) Cells, molecules and morphogenesis: the making of the vertebrate ear. Brain Res 1091:151–171.

Fritzsch B, Beisel KW, Pauley S, Soukup G (2007) Molecular evolution of the vertebrate mechanosensory cell and ear. Int J Dev Biol 51:663–678.

Gross J, Machulik A, Moller R, Fuchs J, Amarjargal N, Ungethüm U, Kuban RJ, Szczepek AJ, Haupt H, Mazurek B (2008) mRNA expression of members of the IGF system in the organ of Corti, the modiolus and the stria vascularis of newborn rats. Growth Factors 26:180–191.

Haas P, Gilmour D (2006) Chemokine signaling mediates self-organizing tissue migration in the zebrafish lateral line. Dev Cell 10:673–680.

Harris JA, Cheng AG, Cunningham LL, MacDonald G, Raible DW, Rubel EW (2003) Neomycin-Induced hair cell death and rapid regeneration in the lateral line of zebrafish (Danio rerio). J Assoc Res Otolaryngol 4:219–234.

Hernández PP, Olivari FA, Sarrazin AF, Sandoval PC, Allende ML (2007) Regeneration in zebrafish lateral line neuromasts: Expression of the neural progenitor cell marker sox2 and proliferation-dependent and-independent mechanisms of hair cell renewal. Dev Neurobiol 67:637–654.

Hertzano R, Montcouquiol M, Rashi-Elkeles S, Elkon R, Yücel R, Frankel WN, Rechavi G, Möröy T, Friedman TB, Kelley MW, Avraham KB (2004) Transcription profiling of inner ears from Pou4f3ddl/ddl identifies Gfi1 as a target of the Pou4f3 deafness gene. Hum Mol Genet 13:2143–2153.

Higgs DM, Souza MJ, Wilkins HR, Presson JC, Popper AN (2002) Age- and size-related changes in the inner ear and hearing ability of the adult zebrafish (Danio rerio). J Assoc Res Otolaryngol 3:174–184.

't Hoen PAC, Ariyurek Y, Thygesen HH, Vreugdenhil E, Vossen RHAM, de Menezes RX, Boer JM, van Ommen GB, den Dunnen JT (2008) Deep sequencing-based expression analysis shows major advances in robustness, resolution and inter-lab portability over five microarray platforms. Nucleic Acids Res 36:e141.

Holley MC, Kneebone A, Milo M (2007) Information for gene networks in inner ear development: a study centered on the transcription factor gata2. Hear Res 227:32–40.

Jiang H, Patel PH, Kohlmaier A, Grenley MO, McEwen DG, Edgar BA (2009) Cytokine/Jak/Stat signaling mediates regeneration and homeostasis in the Drosophila midgut. Cell 137:1343–1355.

Jin X, Zimmers TA, Perez EA, Pierce RH, Zhang Z, Koniaris LG (2006) Paradoxical effects of short- and long-term interleukin-6 exposure on liver injury and repair. Hepatology 43:474–484.

Jones JE, Corwin JT (1996) Regeneration of sensory cells after laser ablation in the lateral line system: hair cell lineage and macrophage behavior revealed by time-lapse video microscopy. J Neurosci 16:649–662.

Kassen SC, Ramanan V, Montgomery JE, T Burket C, Liu CG, Vihtelic TS, Hyde DR (2007) Time course analysis of gene expression during light-induced photoreceptor cell death and regeneration in albino zebrafish. Dev Neurobiol 67:1009–1031.

Kassen SC, Thummel R, Campochiaro LA, Harding MJ, Bennett NA, Hyde DR (2009) CNTF induces photoreceptor neuroprotection and Müller glial cell proliferation through two different signaling pathways in the adult zebrafish retina. Exp Eye Res 88:1051–1064.

Kratz E, Eimon PM, Mukhyala K, Stern H, Zha J, Strasser A, Hart R, Ashkenazi A (2006) Functional characterization of the Bcl-2 gene family in the zebrafish. Cell Death Differ 13:1631–1640.

Leonard WJ, O'Shea JJ (1998) Jaks and STATs: biological implications. Annu Rev Immunol 16:293–322.

Liang J, Burgess SM (2009) Gross and fine dissection of inner ear sensory epithelia in adult zebrafish (Danio rerio). J Vis Exp 27:1211.

Lim DJ (1976) Ultrastructural cochlear changes following acoustic hyperstimulation and ototoxicity. Ann Otol Rhinol Laryngol 85:740–751.

Liu H, Ma Y, Cole SM, Zander C, Chen KH, Karras J, Pope RM (2003) Serine phosphorylation of STAT3 is essential for Mcl-1 expression and macrophage survival. Blood 102:344–352.

Lombarte A, Yan HY, Popper AN, Chang JS, Platt C (1993) Damage and regeneration of hair cell ciliary bundles in a fish ear following treatment with gentamicin. Hear Res 64:166–174.

Ma EY, Rubel EW, Raible DW (2008) Notch signaling regulates the extent of hair cell regeneration in the zebrafish lateral line. J Neurosci 28:2261–2273.

McGill TJ, Schuknecht HF (1976) Human cochlear changes in noise induced hearing loss. Laryngoscope 86:1293–1302.

McHenry MJ, Feitl KE, Strother JA, Van Trump WJ (2009) Larval zebrafish rapidly sense the water flow of a predator's strike. Biol Lett 5:477–479.

Millimaki BB, Sweet EM, Dhason MS, Riley BB (2007) Zebrafish atoh1 genes: classic proneural activity in the inner ear and regulation by Fgf and Notch. Development 134:295–305.

Montgomery J, Carton G, Voigt R, Baker C, Diebel C (2000) Sensory processing of water currents by fishes. Philos Trans R Soc Lond B Biol Sci 355:1325–1327.

Morrissy AS, Morin RD, Delaney A, Zeng T, McDonald H, Jones S, Zhao Y, Hirst M, Marra MA (2009) Next-generation tag sequencing for cancer gene expression profiling. Genome Res 19:1825–1835.

Nicolson T (2005) The genetics of hearing and balance in zebrafish. Annu Rev Genet 39:9–22.

Oates AC, Wollberg P, Pratt SJ, Paw BH, Johnson SL, Ho RK, Postlethwait JH, Zon LI, Wilks AF (1999) Zebrafish stat3 is expressed in restricted tissues during embryogenesis and stat rescues cytokine signaling in a STAT1-deficient human cell line. Dev Dyn 215:352–370.

Oxtoby E, Jowett T (1993) Cloning of the zebrafish krox-20 gene (krx-20) and its expression during hindbrain development. Nucleic Acids Res 21:1087–1095.

Parinov S, Kondrichin I, Korzh V, Emelyanov A (2004) Tol2 transposon-mediated enhancer trap to identify developmentally regulated zebrafish genes in vivo. Dev Dyn 231:449–459.

Qin HR, Kim HJ, Kim JY, Hurt EM, Klarmann GJ, Kawasaki BT, Duhagon Serrat MA, Farrar WL (2008) Activation of signal transducer and activator of transcription 3 through a phosphomimetic Serine 727 promotes prostate tumorigenesis independent of Tyrosine 705 phosphorylation. Cancer Res 68:7736–7741.

Qin Z, Barthel LK, Raymond PA (2009) Genetic evidence for shared mechanisms of epimorphic regeneration in zebrafish. Proc Natl Acad Sci U S A 106:9310–9315.

Raz R, Lee CK, Cannizzaro LA, d'Eustachio P, Levy DE (1999) Essential role of STAT3 for embryonic stem cell pluripotency. Proc Natl Acad Sci U S A 96:2846–2851.

Riehle KJ, Campbell JS, McMahan RS, Johnson MM, Beyer RP, Bammler TK, Fausto N (2008) Regulation of liver regeneration and hepatocarcinogenesis by suppressor of cytokine signaling 3. J Exp Med 205:91–103.

Roberson DW, Rubel EW (1994) Cell division in the gerbil cochlea after acoustic trauma. Am J Otol 15:28–34.

Sano S, Itami S, Takeda K, Tarutani M, Yamaguchi Y, Miura H, Yoshikawa K, Akira S, Takeda J (1999) Keratinocyte-specific ablation of Stat3 exhibits impaired skin remodeling, but does not affect skin morphogenesis. EMBO J 18:4657–4668.

Schebesta M, Lien C, Engel FB, Keating MT (2006) Transcriptional profiling of caudal fin regeneration in zebrafish. ScientificWorldJournal 6 [Suppl 1]:38–54.

Schuck JB, Smith ME (2009) Cell proliferation follows acoustically-induced hair cell bundle loss in the zebrafish saccule. Hear Res 253:67–76.

Sepich DS, Calmelet C, Kiskowski M, Solnica-Krezel L (2005) Initiation of convergence and extension movements of lateral mesoderm during zebrafish gastrulation. Dev Dyn 234:279–292.

Siddiquee K, Zhang S, Guida WC, Blaskovich MA, Greedy B, Lawrence HR, Yip ML, Jove R, McLaughlin MM, Lawrence NJ, Sebti SM, Turkson J (2007) Selective chemical probe inhibitor of Stat3, identified through structure-based virtual screening, induces antitumor activity. Proc Natl Acad Sci U S A 104:7391–7396.

Smith ME, Coffin AB, Miller DL, Popper AN (2006) Anatomical and functional recovery of the goldfish (Carassius auratus) ear following noise exposure. J Exp Biol 209:4193–4202.

Soucek S, Michaels L, Frohlich A (1986) Evidence for hair cell degeneration as the primary lesion in hearing loss of the elderly. J Otolaryngol 15:175–183.

Stone JS, Rubel EW (1999) Delta1 expression during avian hair cell regeneration. Development 126:961–973.

Stone JS, Cotanche DA (2007) Hair cell regeneration in the avian auditory epithelium. Int J Dev Biol 51:633–647.

Taub R (2004) Liver regeneration: from myth to mechanism. Nat Rev Mol Cell Biol 5:836–847.

Thisse B, Thisse C (2004) Fast release clones: a high throughput expression analysis. ZFIN Direct Data Submission. Available at: http://zfin.org/cgi-bin/webdriver?MIval=aa-pubview2.apg&OID=ZDB-PUB-040907-1.

Torbenson M, Yang SQ, Liu HZ, Huang J, Gage W, Diehl AM (2002) STAT-3 overexpression and p21 up-regulation accompany impaired regeneration of fatty livers. Am J Pathol 161:155–161.

Vollrath MA, Kwan KY, Corey DP (2007) The micromachinery of mechanotransduction in hair cells. Annu Rev Neurosci 30:339–365.

Wang H, Park O, Lafdil F, Shen K, Horiguchi N, Yin S, Fu XY, Kunos G, Gao B (2010) Interplay of hepatic and myeloid signal transducer and activator of transcription 3 in facilitating liver regeneration via tempering innate immunity. Hepatology 51:1354–1362.

Wen Z, Zhong Z, Darnell JE Jr (1995) Maximal activation of transcription by statl and stat3 requires both tyrosine and serine phosphorylation. Cell 82:241–250.

Westerfield M (2000) The zebrafish book: a guide to the laboratory use of the zebrafish (Danio Rerio), Ed 4. Eugene, OR: University of Oregon.

Williams JA, Holder N (2000) Cell turnover in neuromasts of zebrafish larvae. Hear Res 143:171–181.

Woods C, Montcouquiol M, Kelley MW (2004) Math1 regulates development of the sensory epithelium in the mammalian cochlea. Nat Neurosci 7:1310–1318.

Wüstefeld T, Rakemann T, Kubicka S, Manns MP, Trautwein C (2000) Hyperstimulation with Interleukin 6 inhibits cell cycle progression after hepatectomy in mice. Hepatology 32:514–522.

Xiao T, Roeser T, Staub W, Baier H (2005) A GFP-based genetic screen reveals mutations that disrupt the architecture of the zebrafish retinotectal projection. Development 132:2955–2967.

Yamashita S, Miyagi C, Carmany-Rampey A, Shimizu T, Fujii R, Schier AF, Hirano T (2002) Stat3 controls cell movements during zebrafish gastrulation. Dev Cell 2:363–375.

Yoshimura A (2009) Regulation of cytokine signaling by the SOCS and Spred family proteins. Keio J Med 58:73–83.

Yu H, Pardoll D, Jove R (2009) STATs in cancer inflammation and immunity: a leading role for STAT3. Nat Rev Cancer 9:798–809.

Zhu BM, Ishida Y, Robinson GW, Pacher-Zavisin M, Yoshimura A, Murphy PM, Hennighausen L (2008) SOCS3 negatively regulates the gp130-STAT3 pathway in mouse skin wound healing. J Invest Dermatol 128: 1821–1829.